Type of file: figure
Label: Supplementary Text and Figures
Filename: Supplimentry Text and Figures.pdf

Supplementary Information

Noninvasive optical inhibition with a red-shifted microbial rhodopsin

Amy S. Chuong, Mitra L. Miri, Volker Busskamp, Gillian A. C. Matthews,
Leah C. Acker, Andreas T. Sørensen, Andrew Young, Nathan C. Klapoetke,
Mike A. Henninger, Suhasa B. Kodandaramaiah, Masaaki Ogawa, Shreshtha B. Ramanlal,
Rachel C. Bandler, Brian D. Allen, Craig R. Forest, Brian Y. Chow, Xue Han, Yingxi Lin,
Kay M. Tye, Botond Roska, Jessica A. Cardin, Edward S. Boyden

Nature Neuroscience: doi:10.1038/nn.3752

Supplementary Figure 1

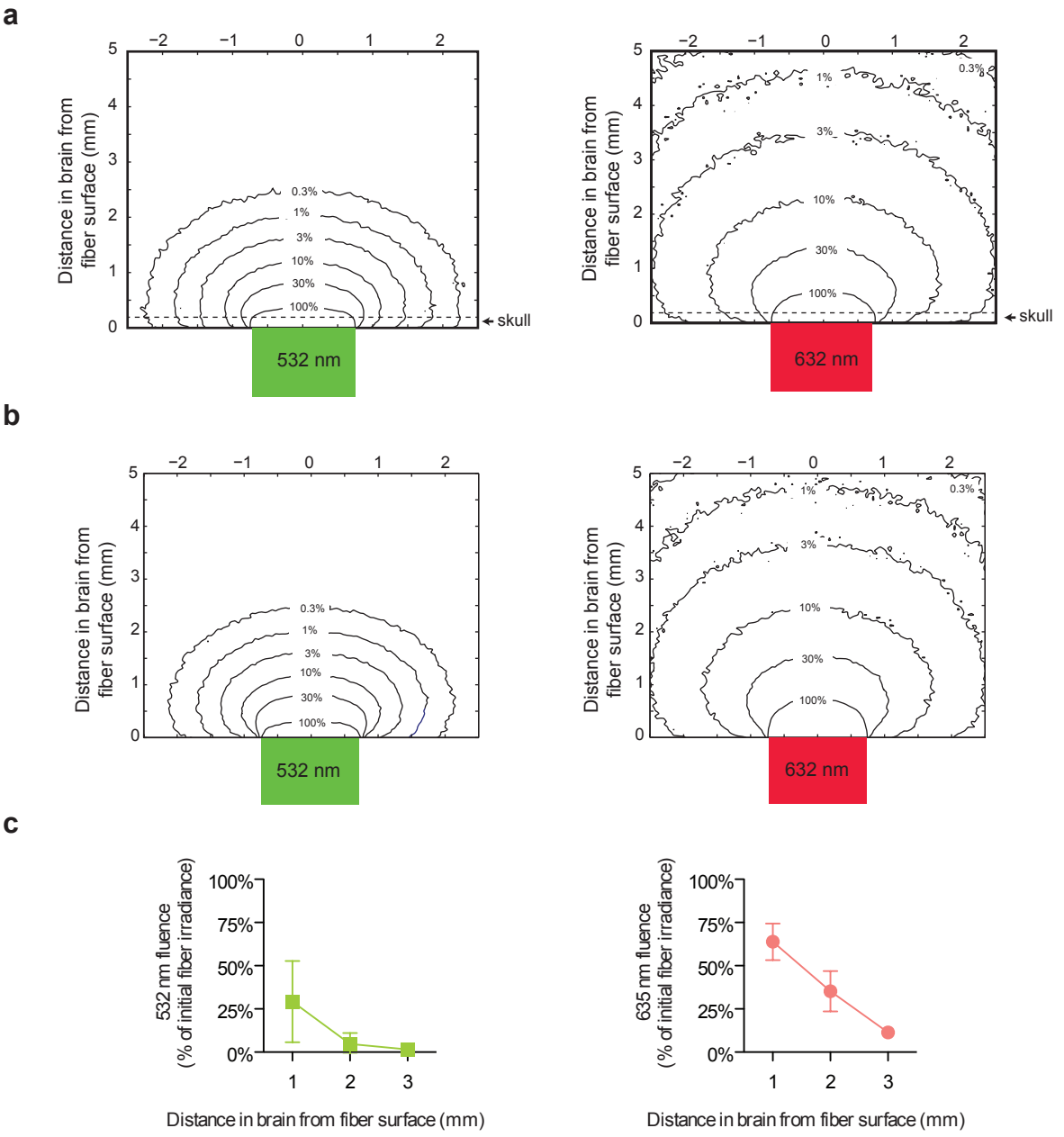

Supplementary Figure 1. Red versus green light propagation. (a) Monte Carlo models of green (*left*, 532 nm) vs. red (*right*, 632 nm) transcranial light propagation into the brain when delivered via a 1500 μm fiber placed on the surface of the skull; the skull is interposed between fiber surface and brain, with skull-brain interface indicated by dotted line. **(b)** Monte Carlo model of green (*left*, 532 nm) vs. red (*right*, 632 nm) transdural light propagation when delivered via a 1500 μm fiber placed on the surface of the brain. **(c)** Relative fluence of green (*left*, 532 nm) vs. red (*right*, 635 nm) light measured in the anesthetized mouse brain when delivered via a 1500 μm fiber placed on the surface of the brain (n = 4 mice for green light; n = 5 mice for red light). Values are means ± standard deviation.

Supplementary Figure 2

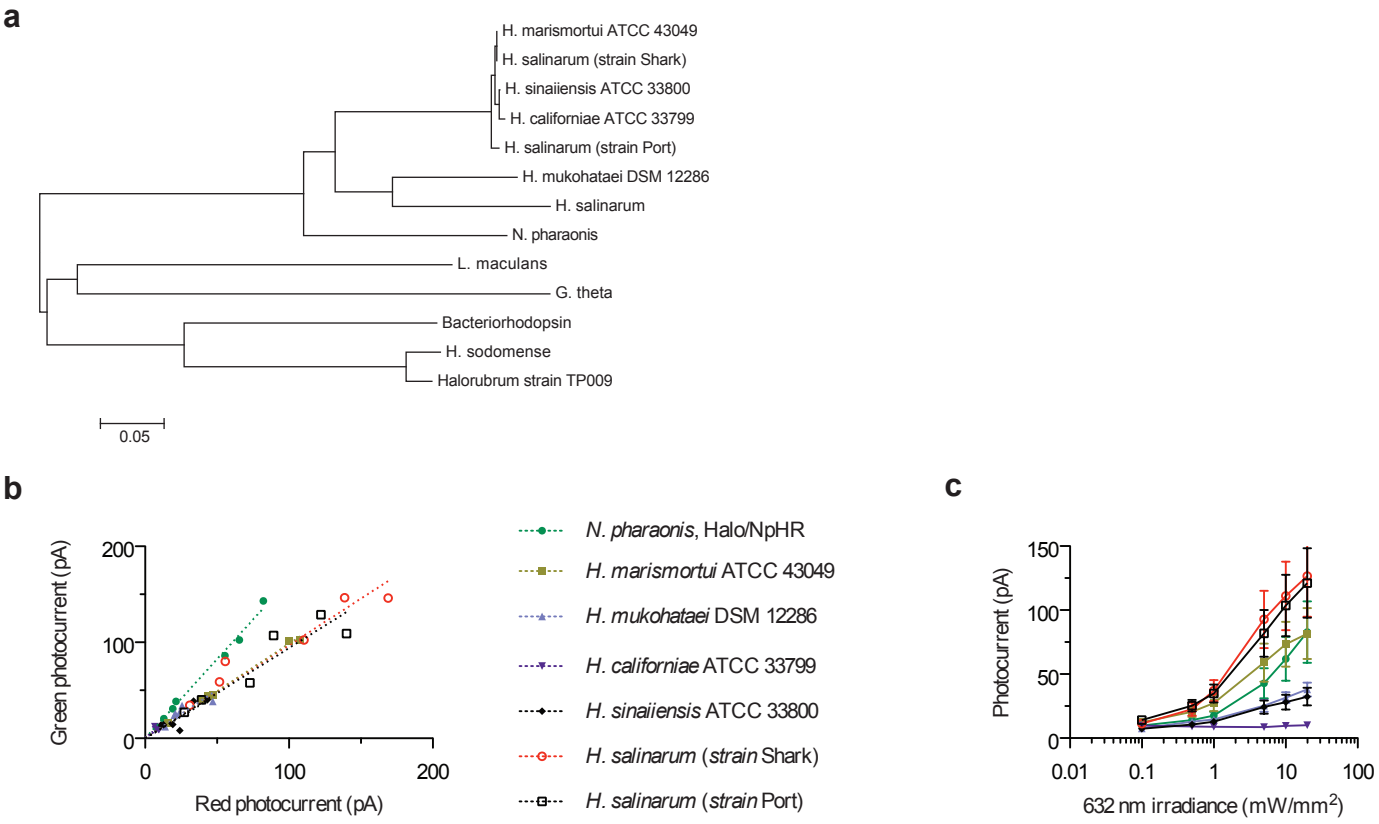

Supplemental Figure 2. Characterization of cruxhalorhodopsin class halorhodopsins.
(a) Cruxhalorhodopsin phylogeny tree. Scale bar indicates number of amino acid substitutions per site. **(b)** Members of the cruxhalorhodopsin class have uniquely red-shifted spectra compared to the *N. pharaonis* halorhodopsin (halo/NpHR), as reflected by red-green photocurrent ratios in cultured cortical neurons. Regressed lines are shown for each opsin, indicating distinct color shifts. (5 mW/mm^2 at 543 or 632 nm). **(c)** Photocurrents of cruxhalorhodopsin class members as a function of red light irradiance (632 nm; n = 6 cells for each opsin). Values are means ± standard error. All measurements were taken in primary hippocampal neuron culture.

Supplementary Figure 3

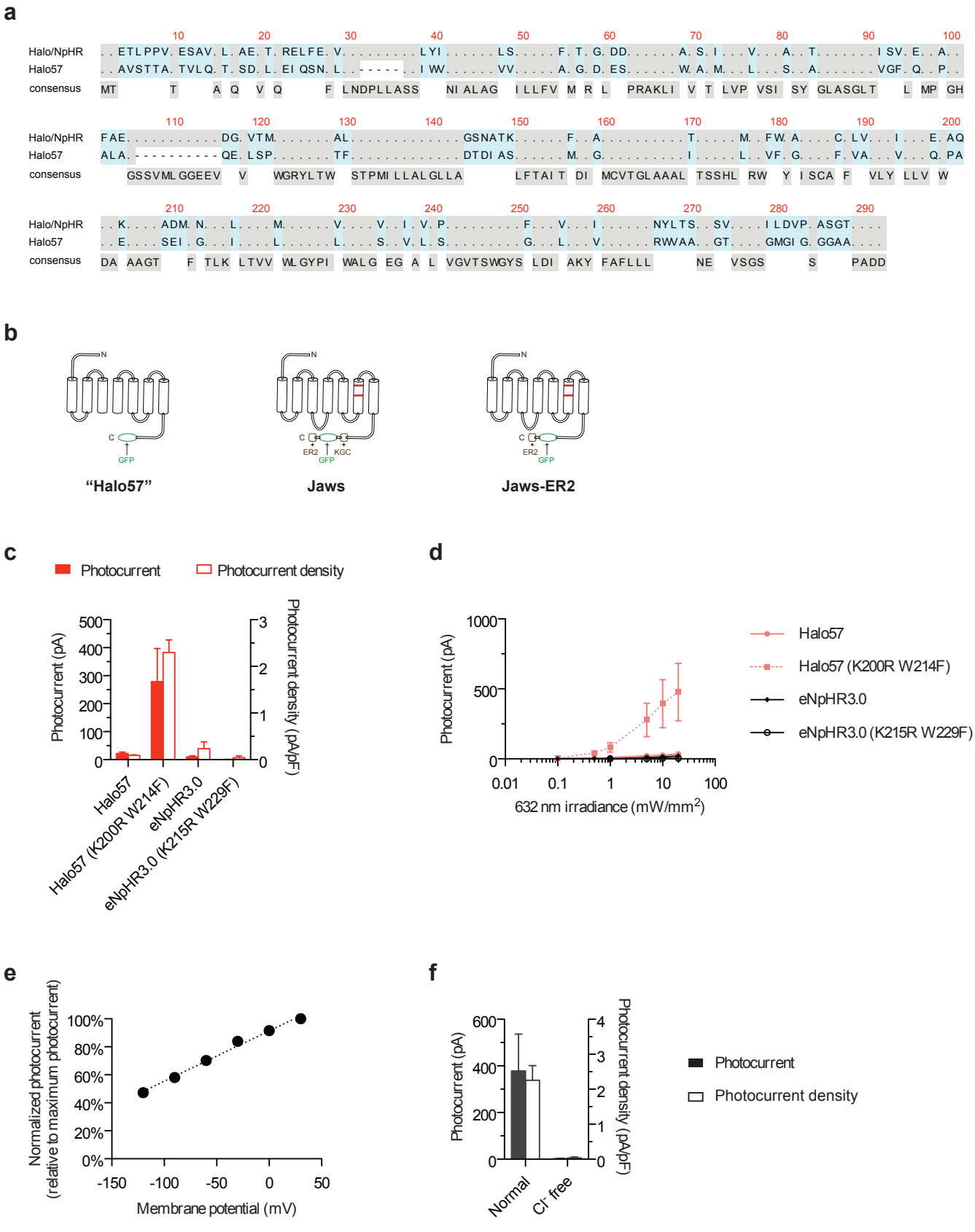

Supplementary Figure 3. Molecular analysis and physiological characterization of Jaws variants. **(a)** Sequence alignment of Halo57, the *H. salinarum* strain shark cruxhalorhodopsin, with the *N. pharaonis* halorhodopsin, demonstrating < 60% sequence homology; blue residues denote sequence divergence, and grey residues, conservation. **(b)** Schematic of Halo57, Jaws, and Jaws-ER2 proteins. Black denotes the Halo57 protein scaffold, red indicates the K200R and W214F point mutations, green indicates the C terminal GFP fusion, and KGC and ER2 respectively refer to endoplasmic reticulum forward transport and Golgi export sequences from the potassium channel Kir2.1. **(c-d)** The K200R W214F mutation boosts Halo57 photocurrents (n = 3 cells for wildtype, n = 6 cells for K200R W214F mutant), but the homologous K215R W229F mutations cause no effect in eNpHR3.0 at 5 mW/mm^2 (**c**) or across a range of 632 nm light powers (**d**; n = 3 cells for both wildtype and mutant eNpHR3.0). **(e)** Current-voltage relationship for light-activated Jaws photocurrents (n = 5 cells; 632 nm, 5 mW/mm^2). Error bars are smaller than the symbols plotted. **(f)** Jaws photocurrent is dependent on $[Cl^-]$ in the extracellular bath solution (n = 3-5 cells; 632 nm, 5 mW/mm^2). All measurements were taken in HEK293FT cells; values are mean ± standard error.

Supplementary Figure 4

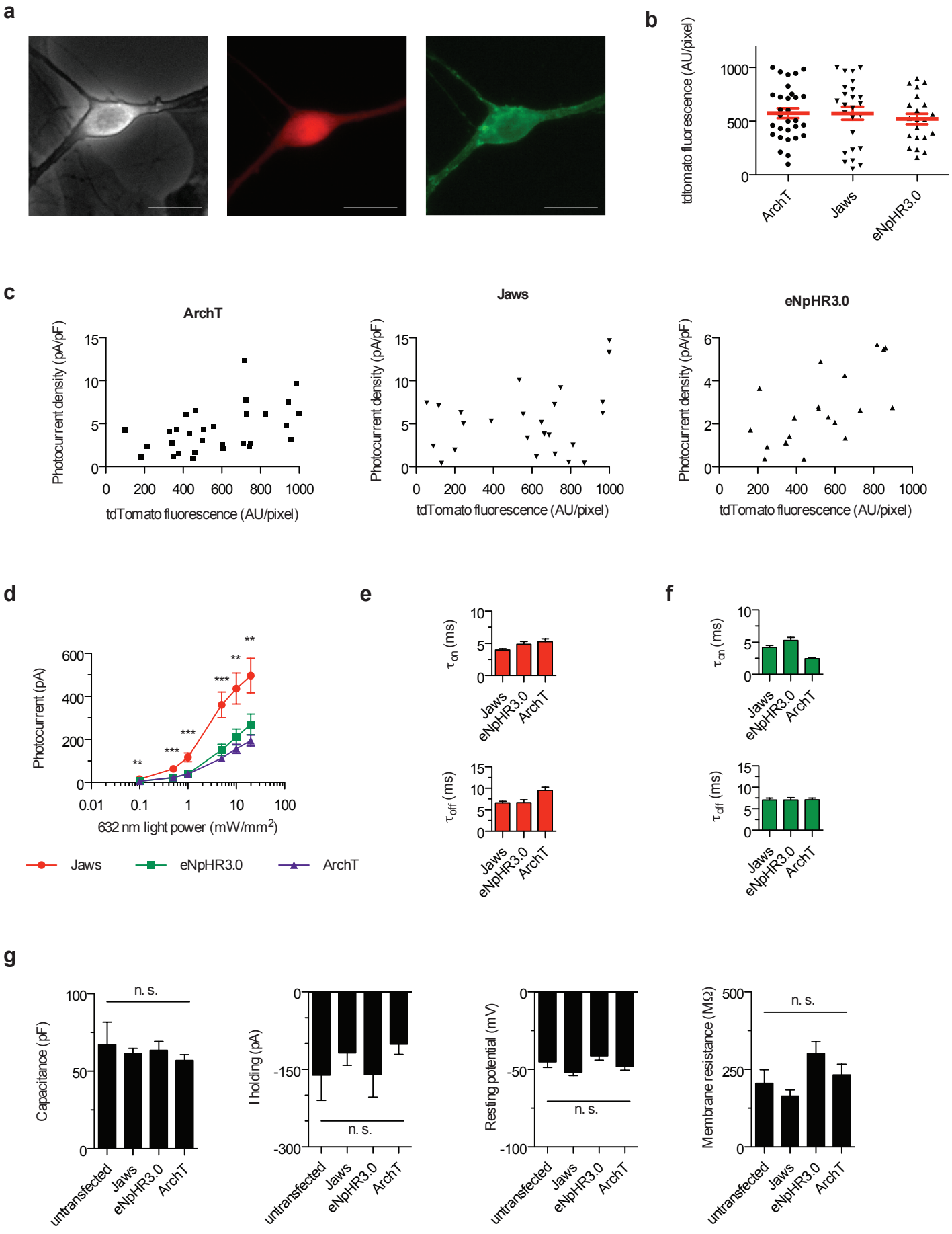

Nature Neuroscience: doi:10.1038/nn.3752

Supplementary Figure 4. Side-by-side comparison of different hyperpolarizing opsins.
(a) Representative phase contrast (*left*), tdTomato (*middle*) and GFP (*right*) images of a tdTomato and opsin-GFP fusion transfected neuron in culture. Scale bar is 50 μm. **(b-c)** Pooled tdTomato fluorescence (**b**) as well as plotted vs. photocurrent density (**c**) for ArchT (*left*), Jaws (*middle*), and eNpHR3.0 (*right*). Photocurrents were measured at 5 mW/mm^2; 632 nm for Jaws (n = 26 cells) and eNpHR3.0 (n = 21 cells), and at 543 nm for ArchT (n = 30 cells). **(d)** Photocurrents for Jaws (n = 26 cells), eNpHR3.0 (n = 21 cells) and ArchT (n = 30 cells) as a function of red light irradiance (632 nm) as measured in transfected neuron culture. **(e-f)** Comparison of hyperpolarizing opsin on-kinetics and off-kinetics using red or green illumination for Jaws (n = 24 cells), eNpHR3.0 (n = 20 cells) or ArchT (n = 29 cells). **(g)** Neuron properties upon opsin expression in culture for Jaws (n = 33 cells), ArchT (n = 36 cells), and eNpHR3.0 (n = 29 cells) as compared to untransfected cells (n = 15), including cell membrane capacitance, holding current when held at -65 mV, resting potential, and cell input resistance. Values are means ± standard error. Statistics for panels d and h: ** $P < 0.01$, *** $P < 0.001$. Panel d was an ANOVA with a Newman-Keuls post hoc test, panel g was an ANOVA with Dunnett's post hoc test using untransfected neurons as the reference. In d, $P < 0.001$ for ArchT and eNpHR3.0, < 0.01 for ArchT and eNpHR3.0, < 0.001 for ArchT and eNpHR3.0, < 0.001 for ArchT and eNpHR3.0, < 0.001 for ArchT and eNpHR3.0, < 0.001 for ArchT and < 0.01 for eNpHR3.0, and < 0.001 for ArchT and < 0.01 for eNpHR3.0 from lowest to highest irradiance; all P values here are computed with a Newman-Keuls post hoc test versus Jaws.

Supplementary Figure 5

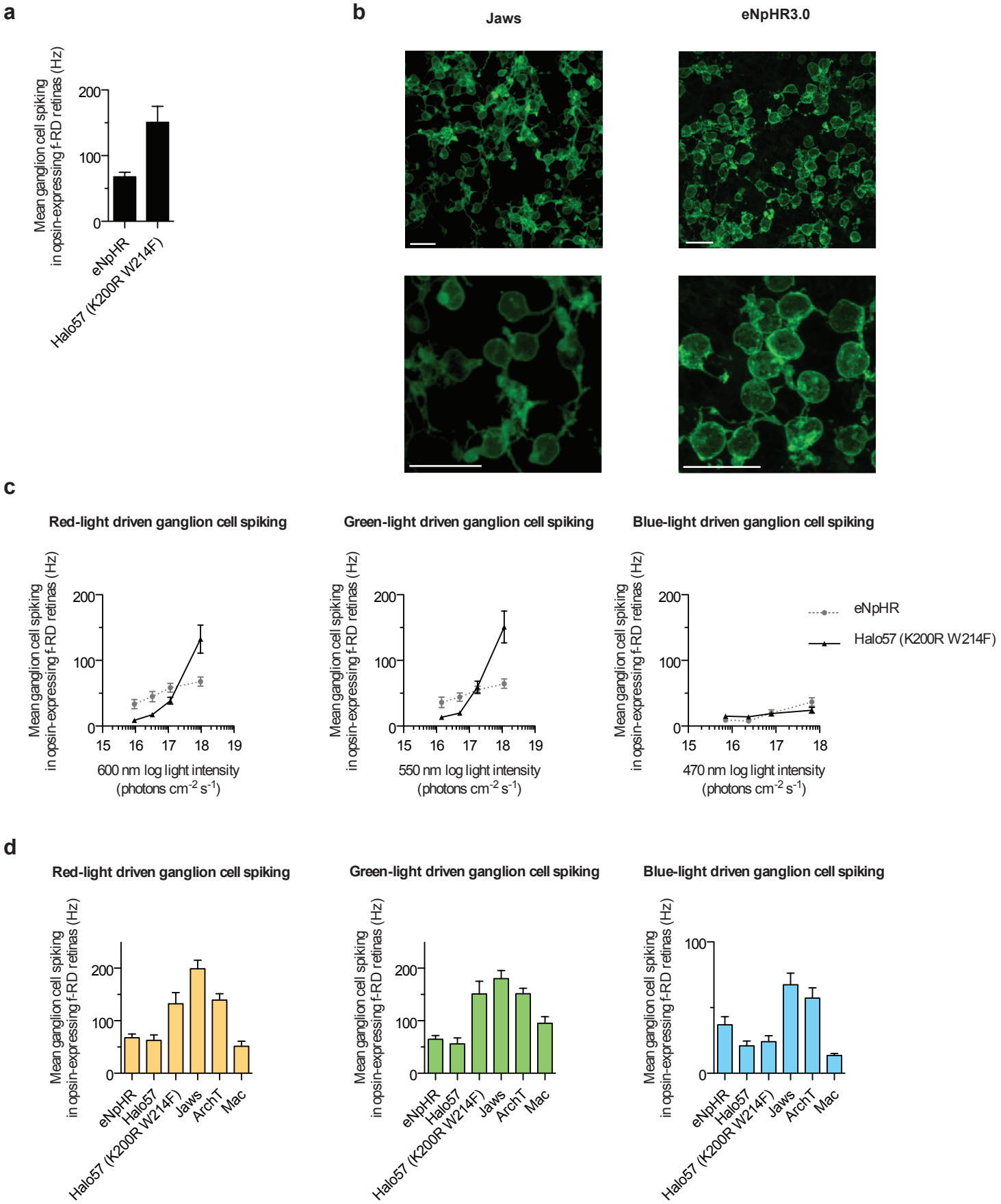

Supplementary Figure 5. Light responses mediated by cone expression and illumination of Halo57 (K200R W214F) in murine retinitis pigmentosa retinas. (a) Comparison of mean spiking for Halo57 (K200R W214F) mutant (n = 16) in ganglion cells downstream from opsin-expressing neurons (9.6 x 10^{17} photons cm^{-2} s^{-1} at 600 nm), using AAV with the mCAR promoter and serotype 8, ~40 days post infection. **(b)** Confocal fluorescence images of Jaws-GFP (*left*) and eNpHR3.0-expressing (*right*) f-RD retinas. Scale bars 20 μm. **(c)** Retinal ganglion cell spike rates vs. red (*left*), green (*middle*), and blue (*right*) irradiances, comparing Halo57 (K200R W214F) vs. eNpHR. **(d)** Comparison of retinal ganglion cell spiking under red, green, and blue illumination for eNpHR (n = 21 cells), Halo57 (n = 14 cells), Halo57 (K200R W214F) (n = 16 cells), Jaws (n = 27 cells), ArchT (n = 30 cells) or Mac (n = 13 cells) expressed in mouse cone cells (light intensity was 6.7 x 10^{17} photons cm^{-2} s^{-1} at 470 nm, 1.2 x 10^{18} photons cm^{-2} s^{-1} at 550 nm, and 9.6 x 10^{17} photons cm^{-2} s^{-1} at 600 nm). Values are means ± standard error.

Nature Neuroscience: doi:10.1038/nn.3752

Supplementary Figure 6

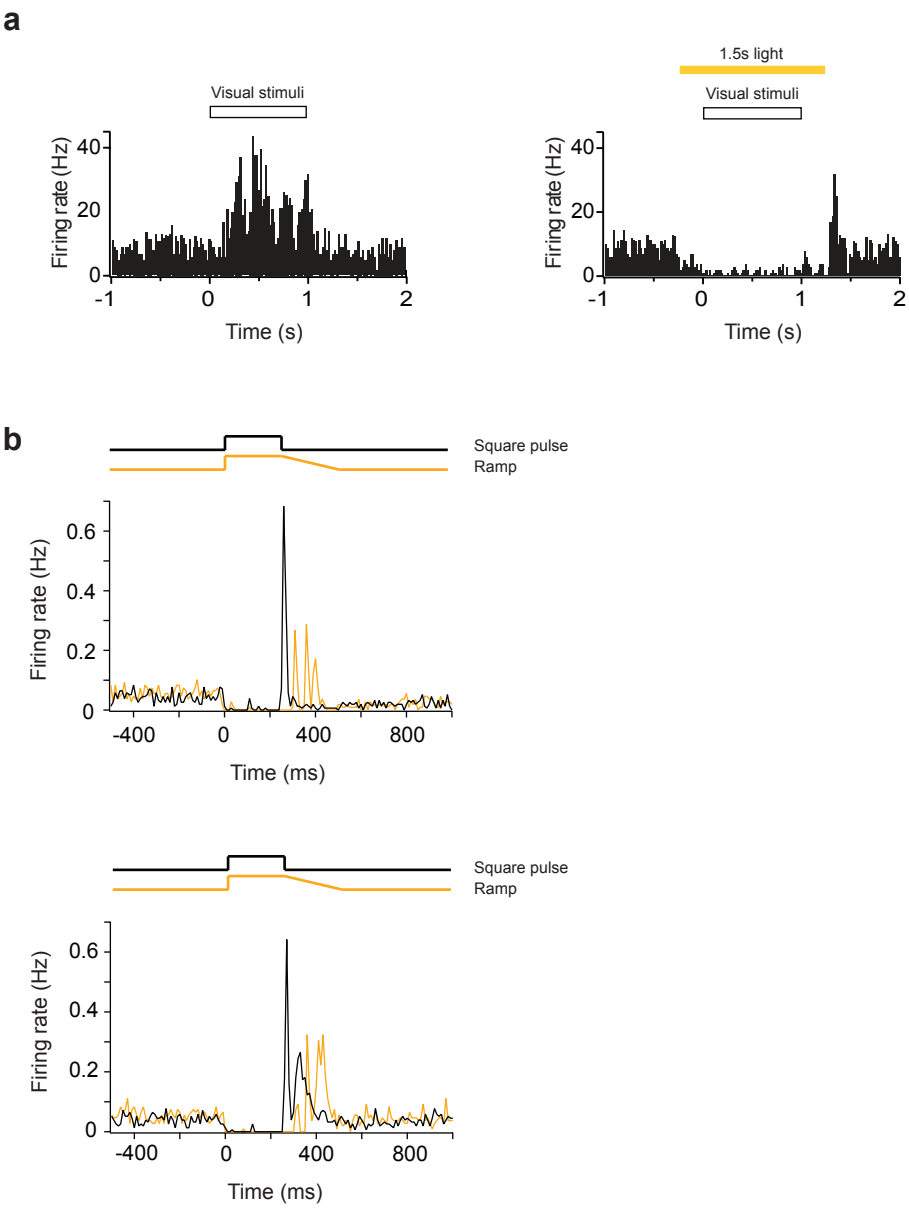

Supplementary Figure 6. Jaws shuts down fast-firing interneurons in visual cortex.
(a) Post-stimulus time histograms for a putative fast-spiking interneuron in the visual cortex of an anesthetized PV-Cre mouse injected with AAV5-FLEX-Jaws virus (35 mW/mm^2 at 593 nm using a 200 µm fiber) undergoing visual stimulation (*left*) and Jaws-mediated inhibition of a visually evoked response (*right*). **(b)** Post-stimulus time histogram for a standard step light pulse (black line) versus ramped illumination (yellow line), for two spontaneously firing visual cortex neurons.

Supplementary Figure 7

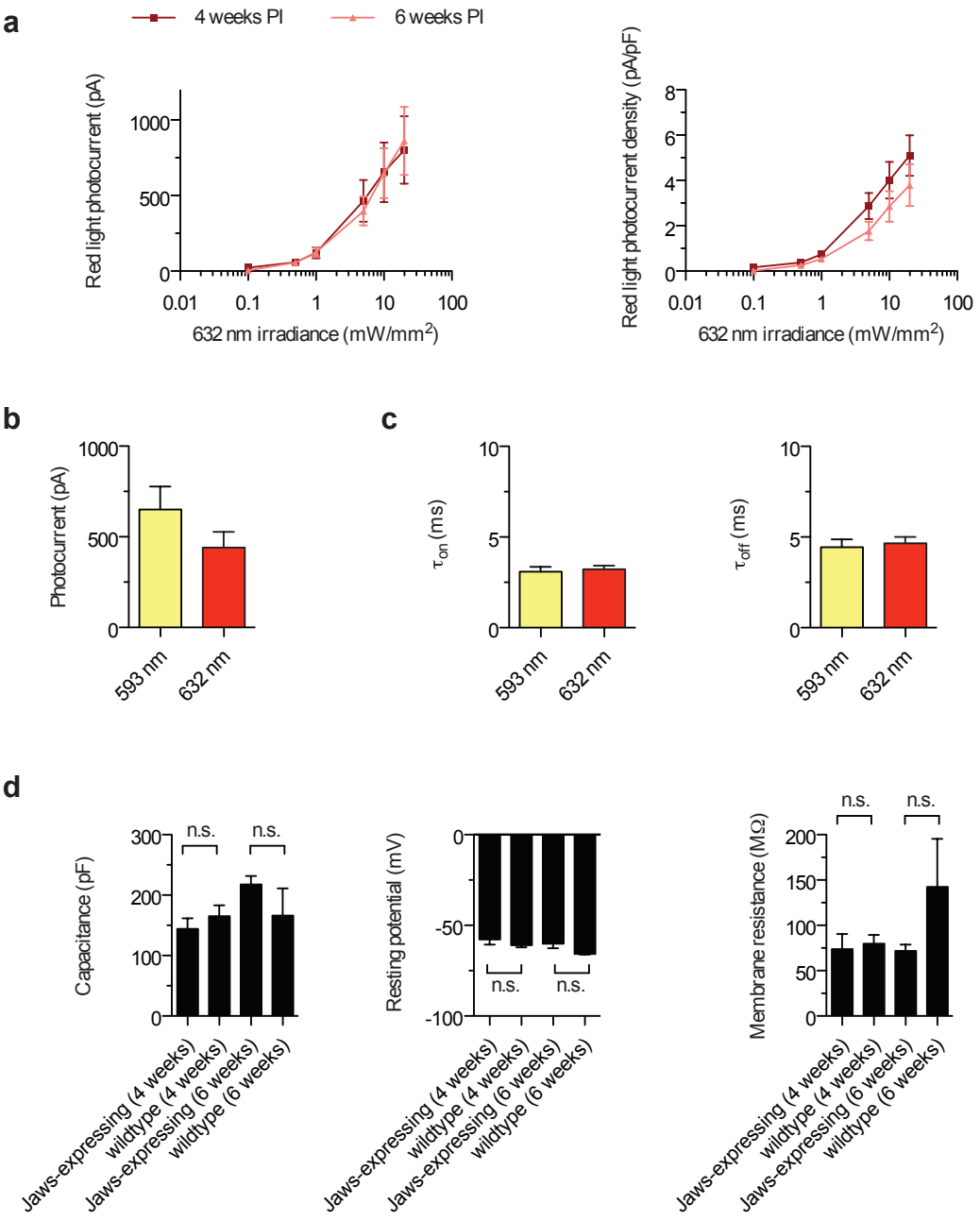

Supplementary Figure 7. ***Ex vivo*** **characterization of Jaws in acute motor cortex slice.**
(a) Jaws photocurrents (*left*) and photocurrent densities (*right*), measured as a function of red light irradiance, were the same at 4 and 6 weeks post-injection in acute slice (n = 8 cells for each timepoint). **(b)** Jaws yellow and red light photocurrents (n = 16 cells, 5 mW/mm^2, 593 or 632 nm). **(c)** Comparison of Jaws on-kinetics (*left*) and off-kinetics (*right*) using red or yellow illumination (n = 16 cells for each, 5 mW/mm^2 593 or 632 nm). **(d)** Neuron properties upon Jaws expression at 4 (n = 9 cells) or 6 weeks (n = 10 cells) post-injection in acute cortical slice as compared against non-opsin-expressing neurons (n = 5 cells at 4 weeks, n = 3 cells at 6 weeks), including cell membrane capacitance (*left*), resting potential (*middle*), and cell input resistance (*right*). Values are means ± standard error. Statistics for panel d: * $P < 0.05$. Panel d was an ANOVA with Dunnett's post hoc test using non-opsin expressing neurons as the reference.

Supplementary Figure 8

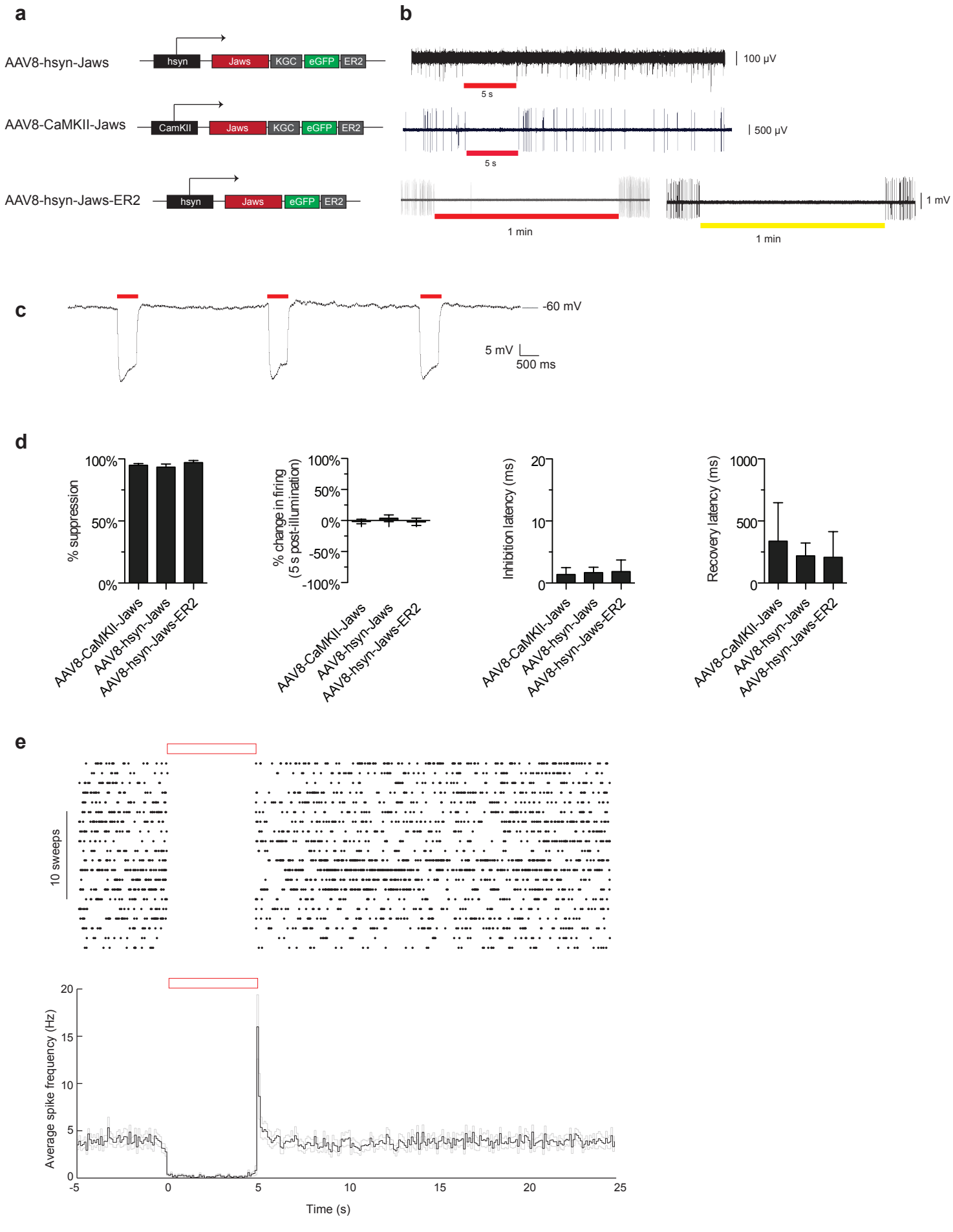

Nature Neuroscience: doi:10.1038/nn.3752

Supplementary Figure 8. Demonstration of Jaws functionality in awake mouse cortex, using invasive 200-µm fibers. (a-b) Gene schematic (**a**) and corresponding representative glass pipette extracellular recording (**b**) of different Jaws variants expressed in cortical neurons 6 weeks post-injection in awake mice undergoing red or yellow light illumination (637 or 593 nm, ~130 mW/mm^2 out the fiber tip). **(c)** Light-induced hyperpolarization of a Jaws-expressing neuron patched in the motor cortex of an anesthetized mouse (AAV8-CAG-Jaws; 635 nm; ~130 mW/mm^2 out the fiber tip terminating ~500 µm above the electrode tip). **(d)** Comparison of different Jaws variants 1-3 months post-injection, as measured by suppression of spontaneous firing, change in firing 5-seconds post-illumination, inhibition latency, and recovery latency (n = 14 units for AAV8-CaMKII-Jaws, n = 17 units for AAV8-hSyn-Jaws, n = 6 units for AAV8-hSyn-Jaws-ER2). **(e)** Spike rasters recorded from a representative neuron (*top*), and population average (*bottom*; n = 31 units) of instantaneous firing rate in neurons showing any degree of light-induced suppression, recorded in awake headfixed mice 4-8 weeks after injection of AAV8 encoding Jaws under either the CaMKII (n = 14 units) or synapsin promoter (n = 17 units; black line, mean; grey lines, mean ± s.e.). Values are means ± standard error.

Supplementary Figure 9

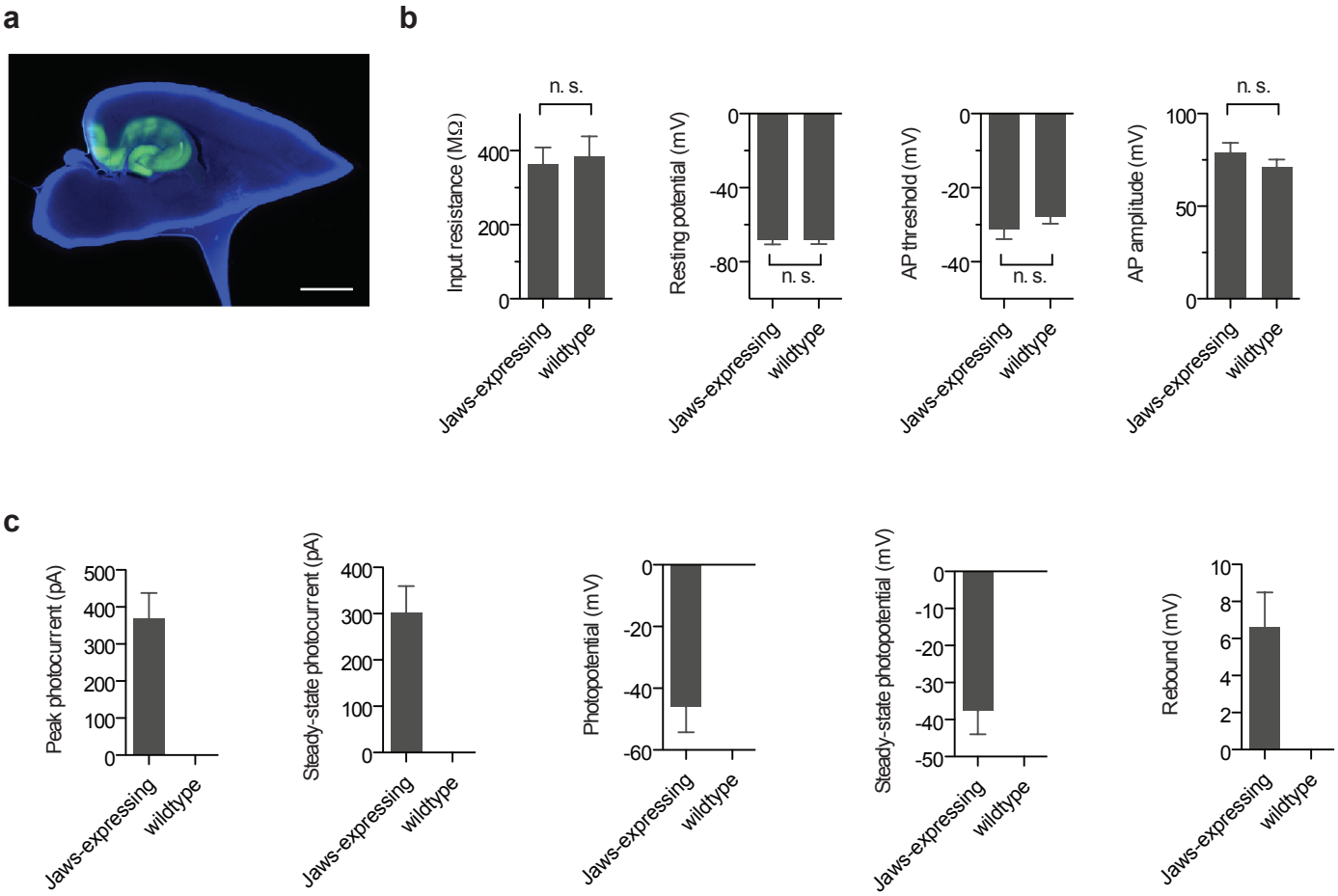

Supplementary Figure 9. ***Ex vivo*** **characterization of Jaws-expressing dentate granule cells in acute hippocampal slice.** **(a)** Epifluorescence image from Jaws-GFP expressing hippocampus, 4 weeks post-injection. Blue indicates DAPI staining, green indicates GFP fluorescence. Scale bar, 1 mm. **(b)** Physiological properties upon opsin expression at 4 weeks post-injection in dentate granule cells, including cell input resistance, resting potential, electrically evoked action potential threshold, electrically evoked action potential amplitude. **(c)** Physiological properties for Jaws-expressing and wildtype dentate granule cells upon red light illumination, including peak and steady-state photocurrent, peak and steady-state photopotential, and post-illumination rebound voltages. n = 12 for Jaws-positive cells, n = 15 for wildtype cells, throughout this panel. Illumination was 1 second at 68 mW/mm^2, 625 nm. Values are means ± standard error. Statistics for panel b: * $P < 0.05$. Panel b was a Student's t-test.

Supplementary Table 1

Strain	Age (d)	Gender	AAV incubation (d)	Opsin	Multi-electrode array recordings of the retinal ganglion cells
f-RD (C3H)	71	F	36	eNpHR	recordings
f-RD (C3H)	74	F	36	Halo57	recordings
f-RD (C3H)	75	F	37	Halo57 (K200R W214F)	recordings
f-RD (C3H)	64	F	34	ArchT	recordings
f-RD (C3H)	67	F	33	Mac	recordings
f-RD (C3H)	67	F	33	Mac	recordings
f-RD (C3H)	65	F	29	Jaws	recordings
f-RD (C3H)	50	F	22	eNpHR3.0	no response (patch clamp recordings of cones revealed tiny photocurrents; data not shown; n = 4 retinas)
s-RD	113	F	21	eNpHR3.0	no response (patch-clamping was not tried; n = 3 retinas)